RSC Advances

PAPER

View Article Online
View Journal | View Issue

Cite this: *RSC Adv.*, 2021, **11**, 27541

Ball-lens assisted sensitivity improvement of fluorescence immunoassay in microchannels†

Qingquan Zhang,‡[a] Jiajia Li,‡[a] Yuting Su,[a] Xiaoyan Pan[b] and Hongwei Gai *[a]

Received 6th June 2021
Accepted 4th August 2021

DOI: 10.1039/d1ra04360a

rsc.li/rsc-advances

The relatively low sensitivity is the limitation of ELISA in early screening of diseases. Various signal enhancing methods are developed to increase detection sensitivity, but most of them require professional operation and are not compatible with commercial reagent kits or automatic analysis instruments, limiting their application in clinical testing. Here, we present a contactless and user-friendly ball-lens assisted fluorescence enhancing (BFE) method to improve immunoassay sensitivity. The BFE effect is observed in experiment and demonstrated by the simulation. Based on the BFE effect, the detection sensitivity of the immunoassay is improved about 3.6-fold and the limit of detection is lowered by more than 3-fold using commercial reagents and standard ELISA processes. In addition, the BFE effect causes no damage to the linear dependence, specificity and accuracy of clinical plasma measurement. The established method shows a high compatibility with automatic microfluidic immunoassay systems and other signal enhancing techniques, displaying great potential in multi-technique coupling assays and clinical applications.

Introduction

Enzyme-linked immunosorbent assay (ELISA) and its variants are the golden standard for specific protein measurement due to their high specificity, accuracy and straightforward readout.[1] The automatic instruments, standard work-flow and commercial reagent kit enable ELISA to be widely used in clinical testing and biological research,[2] playing a more and more important role in disease screening,[3,4] food safety[5,6] and environmental monitoring.[7,8]

In clinical test, ELISA usually adopts fluorescence or luminescence as detection signal.[9] The fluorescence intensity is decreased with the target protein concentration, which causes ELISA is not able to discover the abnormal expression of proteins at the early stage of diseases.[10] To amplify the fluorescence at low concentration, various fluorescence-signal enhancing approaches are developed, including immuno-PCR,[11,12] quantum dot (QD) labeling,[13,14] plasmon or dielectric resonance enhancing,[15,16] and ultra-small volume confining detection.[17,18] A portion of techniques increase the sensitivity 100–1000 folds and a few LODs reach femtomolar level.[19] However, most methods still exist some drawbacks: (1) the modification of immuno-reagents requires professional operation, which causes measurement deviation from different user (*e.g.* labeling efficiency); (2) process-flow is complicated and unique (*e.g.* particle imaging and counting[20]), which hinders the coupling with automatic system; (3) some signal amplification increase assay time remarkably (*e.g.* PCR). How to improve the sensitivity of fluorescence detection, while maintain ELISA's standard process and automatic operation, is still a challenge.

Microfluidics natively have large specific surface area, fast mass/heat transferring, and precise fluid control, which enable it to be an automatic and high throughput assay platform.[21,22] Immunoassay in microfluidics can reduce reagent consumption, shorten assay time and save manual operation.[23] In comparison with non-microfluidic platform, microfluidics has a unique signal-enhancing approach which is the integration of micro-optics.[24–26] For example, TiO_2 colloids have been used to improve the collection efficiency of rays and single fluorophore images have been captured under a low numerical aperture (NA) objective.[27] Dielectric microspheres integrated into a microchannel have intensified the excitation of QDs and realized the fast detection of single nanoparticle.[28] Recently, Yang *et al.*, have assembled 3 μm melamine microparticles into 3D microstructures as in-site lenses to enhance immunofluorescence.[29] The detection sensitivity has been improved several folds and the LOD of mouse IgG reaches 2 ng mL^{-1}. However, the complicated and subtle assembly process possibly limited its practical value. In addition, the direct contact of particle with solution caused the non-specific protein adsorption and worsen the immunoassay sensitivity.

[a]*Jiangsu Key Laboratory of Green Synthesis for Functional Materials, School of Chemistry and Materials Science, Jiangsu Normal University, Xuzhou, Jiangsu 221116, China. E-mail: gai@jsnu.edu.cn*

[b]*Department of Laboratory Medicine, The Second Affiliated Hospital, Zhejiang University School of Medicine, Hangzhou 310009, China*

† Electronic supplementary information (ESI) available. See DOI: 10.1039/d1ra04360a

‡ These authors contributed equally.

Here, we present a contactless and easy fabrication ball-lens assisted fluorescence enhancing (BFE) method to improve immunoassay sensitivity in the micro-channel. The ball-lens was embedded at the top of the microchannel and insulated from the solution by a PDMS membrane. The fluorescence of different dyes was intensified several folds. Following standard working flow of ELISA, the sensitivity and the limit of detection (LOD) of carcinoembryonic antigen (CEA) measurement were improved significantly by BFE effect, and the specificity and accuracy were maintained as well as ELISA in clinical testing.

Experimental

Materials and equipment

Monoclonal capture antibody (Cab, L1C00202), horseradish peroxidase labeled detection antibody (HRP-Dab, L1C00205H), and human CEA were purchased from Shanghai Linc-Bio Science Co., Ltd. (China). Acid-washed glass beads, Amplex red and 1-ethyl-3-(3-dimethylaminopropyl) carbodiimide hydrochloride (EDC) were purchased from Sigma-Aldrich. Sylgard 184 PDMS oligomer and curing agent were from Dow Corning. Ultra-filters with 100 kDa molecular weight cut-off (Amicon ultra-0.5 mL centrifugal filters) were from Millipore. Barium titanate solid glass microspheres (BTGMs) was from Cospheric (US). Bovine serum albumin (BSA) and hydrogen peroxide were from Shanghai Aladdin Bio-Chem Technology Co., Ltd. (China). 3-Aminopropyltriethoxysilane (APTES), glutaraldehyde, Tween 20, fluorescein sodium, and rhodamine B (Rh B) were obtained from J&K Scientific Ltd (Beijing, China). Dry-film photoresist (ETERTEC BR40120P) was purchased from Eternal Materials Co., Ltd.

An inverted microscope (Olympus IX71) with a 10× objective was from Olympus (Tokyo, Japan), and an Evolve 512 electron-multiplied charge-coupled device was from Photometrics (EMCCD; Tucson, USA). The fluorescence filter combinations are as follows: TXRED-4040B-OMF (exciter: 562/40, emission: 624/40 nm, dichroic mirror: 593 nm) for Rh B and resorufin, and FITC-3540B-OMF (exciter: 482/35, emission: 536/40 nm, dichroic mirror: 506 nm) for fluorescein. 4″ single-sided lithography machine (H94-25C) was purchased from Sichuan Nanguang Vacuum Technology Co., Ltd. Plasma cleaner (PDC-32G-2*) was provided by Harrick Plasma (USA). IEC CL31 Multispeed Centrifuge was from Thermo-Fisher.

Fabrication of microdevice integrated with BTGMs

The microdevice integrated with BTGMs were fabricated following a modified soft photolithography process simply described as follows: the positive photoresist mold was produced based on previous method.[30,31] PDMS precursor was degassed by vacuum and poured onto the positive photoresist mold until the mold was immersed. BTGMs were embedded in the PDMS precursor at the top of photoresist patterns. Then, the mold with PDMS precursor was placed on 80 °C hot plate for 30 minutes. After that, PDMS piece with patterns was peeled off from the mold, punctured reservoirs and bonded to clean glass substrate by oxygen plasma. The microdevice with BTGMs was formed.

The dimensions of the microchannels were 600 μm (width) and 360 μm (height).

Fluorescence measurement with different beads, fluorescent dyes and concentrations

A series of microdevices embedded with BTGMs, whose size were varied from 300 μm to 1000 μm, were fabricated following the above process. 5 μL of 1×10^{-6} M fluorescein solution was pipetted into the microchannels. Then, we captured the fluorescence images of BTGMs one after another by using an inverted fluorescence microscope equipped an EMCCD. The fluorescence intensity of each image was measured by Image J.

5 μL of 1×10^{-7} M rhodamine B (RhB) solution, 5 μL of 3.9×10^{-7} M resorufin solution, and 5 μL of 5×10^{-7} M fluorescein solution were filled in the microchannel with ~700 μm BTGMs in sequence. The fluorescence images of each solution were captured at the locations with and without BTGMs, and the fluorescence intensity was measured by Image J.

0.0 M, 1.9×10^{-7} M, 3.9×10^{-7} M, 7.8×10^{-7} M, 15.5×10^{-7} M and 31.0×10^{-7} M resorufin solution were prepared. These resorufin solutions were filled in the microchannel with ~700 μm BTGMs one after another. Every resorufin solution was observed, and the fluorescence images of BTGMs were captured.

Sandwich immunoassay in the microchannel

The glass substrate was modified by glutaraldehyde as follows: glass slides were cleaned by chromic acid lotion and DI water in sequence. 5% (v/v) APTES solution was prepared by mixing APTES with proper acetone. The clean slides were immersed in 5% (v/v) APTES solution for 30 minutes, washed by acetone, and blow-dried by nitrogen. Then, these slides were immersed in 10% (v/v) glutaraldehyde solution at 37 °C for 1 hour. Then, the slides were washed by DI water and blow-dried by nitrogen. The surface of glass substrate had aldehyde groups. PDMS pieces with BTGMs bonded to aldehyde functionalized substrate to form microchannel for antibody immobilization.

5 μL of 0.7 μg mL^{-1} CAb solution was added into the glutaraldehyde modified microchannel and reacted with aldehyde groups at 4 °C overnight. The free CAbs were removed and the channel was blocked by 4% (wt) BSA solution for 30 minutes. Then, 5 μL of 5 ng mL^{-1} CEA was added in the channel and incubated at room temperature for 30 minutes. After that, the microchannel was washed by a 10 mM phosphate buffer with 137 mM NaCl (PBS, pH 7.4) containing 0.1% (v/v) tween 20 (PBST) three times. 5 μL of 0.3 mg mL^{-1} HRP-DAb solution was incubated in the microchannel for 30 minutes. After washing by PBST, 5 μL of fluorescent substrate solution (A mixture of 25 μM Amplex red and 25 μM hydrogen peroxide with a volume ratio of 1 : 1) was added and reacted for 8 minutes. Then, the microdevice was observed by an inverted fluorescence microscope with a 10× objective lens (NA = 0.3). The fluorescence images were captured by an EMCCD and the intensity was measured by Image J. The antibodies, BSA and Amplex red were dissolved in PBS.

Specificity and matrix effect experiment

5 μL of PBS, 5 μL of CEA (20 ng mL^{-1}), 5 μL of BSA (100 ng mL^{-1}), 5 μL of squamous cell carcinoma antigen (SCCA, 100 ng mL^{-1}), 5 μL of neuronspecific enolase (NSE, 100 ng mL^{-1}), and 5 μL of prostate-specific antigen (PSA, 100 ng mL^{-1}) were filled into six microchannels with immobilized CAbs respectively and incubated for 30 minutes. Then, the microchannels were washed by PBST. 5 μL of 0.3 mg mL^{-1} HRP-DAb solution was added in the microchannel and incubated for 30 minutes. After washing, 5 μL of fluorescent substrate solution was added and incubated for 8 minutes. Then, we captured the fluorescence images of six microchannel at the BTGMs location and measured the fluorescence intensity by Image J.

500 μL of plasma was added in an ultrafilter with a 100 kDa molecular weight cutoff and centrifuged for 15 min (14 000 G). CEA-free plasma was obtained. Then, a portion of CEA-free plasma was diluted by 2-, 4-, and 10-fold respectively to form 100% (v/v), 50% (v/v), 25% (v/v), and 10% (v/v) CEA-free plasmas. These diluted CEA-free plasmas were detected following the established working flow.

Analysis of plasma

The plasma was collected from single-donor, mixed with anti-coagulants, and stored in −20 °C refrigerator. Before analysis, the plasma was diluted two folds by PBS (pH 7.4). The diluted plasmas were measured by a standard addition method. The quantitative data was acquired by Image J.

Results and discussion

BFE effect investigation

The setup to observe BFE effect is shown in Fig. 1A. The fluorescent dye solution was filled in the microchannel. Under the excitation of a mercury lamp, the fluorescence was collected by a 10× objective (NA = 0.3) and imaged by an EMCCD. The microchip integrated with high refractive index beads was fabricated following a modified process flow (Fig. S1, ESI†). Microbeads were embedded on the top of the microchannel and insulated from the solution by a PDMS membrane with a thickness of several micrometers (Fig. 1B and C). When 1 × 10^{-6} M fluorescein solution was in the microchannel, we discovered that the fluorescence image with the bead (Fig. 1D) was brighter than that in the absence of the bead (Fig. 1E), revealing an obvious BFE effect. Meanwhile, the fluorescence image of DI water showed no enhancement (Fig. 1F and G). The BFE effect might be attributed to three aspects: (1) the microbead focused the exciting light and improved the excitation efficiency;[32] (2) the microbead focused the emitted fluorescence and enhanced the local intensity; (3) the microbead improved the fluorescence collection efficiency, especially at high incidence angles, and increased the effective NA of the objective.[33] To verify the BFE effect was really existed or a false phenomenon caused by inappropriate focusing of the objective lens, we investigated the objective lens focusing process (Fig. S2, ESI†). By considering the best focusing position as a center represented as '0' position, we adjusted the focusing

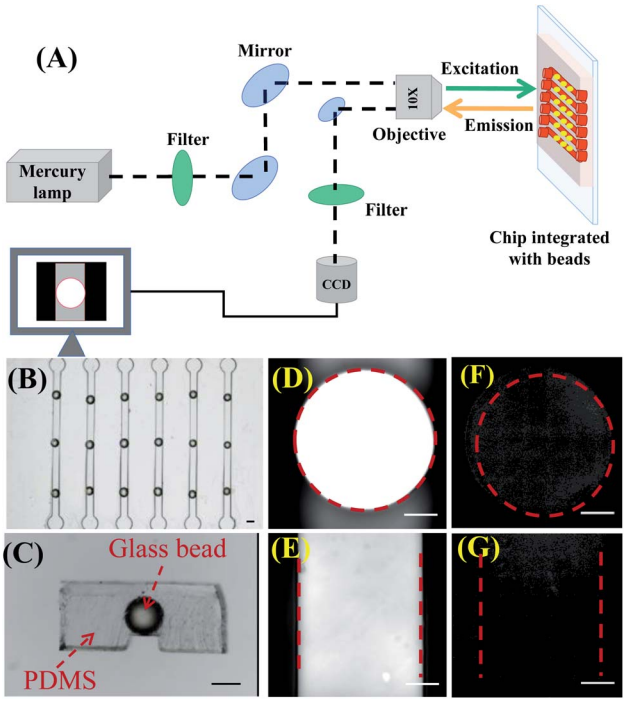

Fig. 1 (A) Setup to test fluorescence enhancing effect. Top (B) and cross-section view (C) of microdevice integrated with microbead. Fluorescence images with microbead (D and F) and in the absence of microbead (E and G). The solution in the microchannel is 1 × 10^{-6} M fluorescein solution (D and E) or DI water (F and G) respectively. Scale bars, 600 μm (B and C) and 160 μm (D–G).

knob with different cycles along the clockwise and anticlockwise direction. The images and quantitative data indicated that the fluorescence intensity was always enhanced by the ball-lens no matter how the focusing position was changed.[34] In addition, we simulated the function of the ball-lens by using ZEMAX software. Rays emitted from the point light source would deflect from the original direction when it passed through the ball-lens (Fig. S3, ESI†). The exit rays would focused before collected by the objective. The rays-focusing effect of the ball-lens could increase the effective collection angle of the objective. By using 700 μm bead ($n = 1.9$) as an example, the collection half angle is increased from ~11.8° (absence of bead) to ~23.1° (with bead) under the 10× objective (NA = 0.3). The enhancement factor (E) was proportional to the square of the numerical aperture and calculated following eqn (1).

$$E = \pi B_0 (\mathrm{NA})^2 \frac{1}{\beta^2} = \pi B_0 (n \sin\theta)^2 \frac{1}{\beta^2} \quad (1)$$

where B_0 is the brightness of the object, β is the magnification of the objective, n is the refractive index. The calculated E was about 3.68.

Influence factors of BFE effect

For a given microchannel, BFE effect might be influenced by the size and the refractive index (RI) of the bead. 1 × 10^{-6} M fluorescein solution was tested. The bead-enhanced fluorescence rose steadily with bead size varied from 300 to 700 μm. This was

resulted from increased effective collection efficiency of rays. Once the bead size exceeded 720 μm, the bead-enhanced fluorescence reduced instead (Fig. 2A), which might be caused by the lowering of the bead transmittance. The optimum bead size was a balance on the transmittance and the collection efficiency of rays. In the microchannel with a width of 600 μm, the highest BFE effect was achieved using ~700 μm beads. From our simulation, RI affected the focusing capability of ball-lens. Here, we chose two kinds of glass beads: common glass beads (RI ~1.5) and BTGMs (RI ~1.9). Under the same conditions (microchannel, dye solution, and bead size), the enhancing factor of BTGMs (RI ~1.9) was obviously larger than that of common glass bead (RI ~1.5) as shown in Fig. 2C. The results coincided with our simulation and the previous reports.[27] Fig. 2B showed the fluorescence enhancement of different dyes. In the same microchannel with BTGMs, the fluorescence of RhB, resorufin and fluorescein solution were enhanced 3.7, 4.0, and 2.4-fold respectively, revealing that the BFE effect was suitable for various fluorescent dyes.

The basis of quantitative analysis was the linear relationship of fluorescence intensity and sample concentration. To evaluate the influence of BFE effect on the linear relationship, we chose resorufin as a model dye, because resorufin was widely used in biochemical analysis. When the resorufin concentration was varied from 0.0 to 31.0 × 10^{-7} M, the fluorescence intensity increased linearly with the concentration whether the bead existed or not (Fig. 2D), which indicated that the linear relationship was not weakened by BFE effect and laid the basis for subsequent immunoassay.

Sensitivity improvement of fluorescence immunoassay in the microchannel

BFE effect was an optical enhancing method requiring no reagent modification and no interference to assay process, which displayed a high compatibility with ELISA and other fluorescence enhancing approaches. Here, immunoassay was carried out in the microchannel following the standard ELISA process, such as CAb immobilization, blocking, antigen and HRP-DAb incubation, *etc.* (Fig. 3A). The immunoreaction parameters were optimized in the microchannel without bead by using 5 ng mL^{-1} CEA as positive control and PBS as blank. Under optimum conditions, standard CEA solutions with different concentrations were detected. Bead-enhanced fluorescence images and original images in the absence of bead were captured and compared from 0 to 70 ng mL^{-1} (Fig. 3B). The quantitative data of fluorescence intensity against CEA concentration were extracted from these images and showed in Fig. 3C. When CEA concentration was varied from 1 to 30 ng mL^{-1}, the detected fluorescence was enhanced by the bead in the range of 1.7–3.2-fold. The slope of the enhanced curve was 3.6-fold larger than that of original curve without bead, revealing that the sensitivity of immuno-fluorescence detection was increased about 3.6-fold by the BFE effect (Fig. 3D). It was noted that the background signal of fluorescence detection was composed of the noise from the detection instrument and non-specific signal from complex sample. The noise from the detection instrument was not affected by BFE effect. The non-specific signal was enhanced by one part of BFE effect (improved collection efficiency of rays). Meanwhile, the target signal was enhanced by all three parts of BFE effect (enhanced excitation, fluorescence focusing and collection efficiency improvement). The enhancing factor of background signal was smaller than that target signal, which resulted in the detection sensitivity was increased.

In addition, the linear relationship of the enhanced curve was as well as that of the original curve. This might be resulted from that the microbead was insulated from solution and the non-specific adsorption at solid/liquid interface was prohibited.

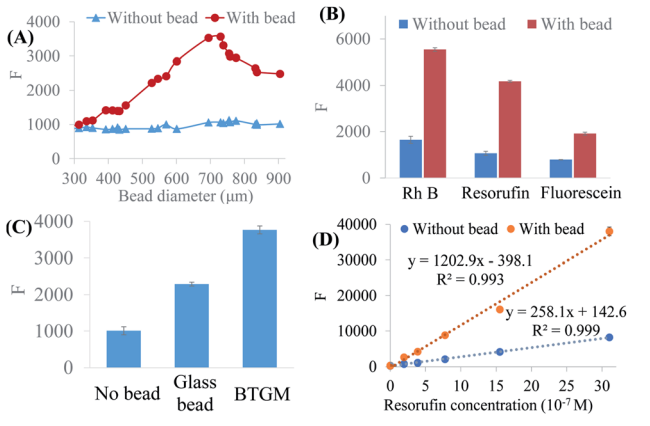

Fig. 2 (A) The influence of the bead diameter on BFE effect. (B) BFE effect of different fluorescent dyes. The concentrations are 1 × 10^{-7} M (Rh B), 3.9 × 10^{-7} M (resorufin) and 5 × 10^{-7} M (fluorescein). (C) Influence of RI on BFE effect. RI is ~1.5 (glass bead) or ~1.9 (BTGM). (D) BFE effect of resorufin solution with different concentrations.

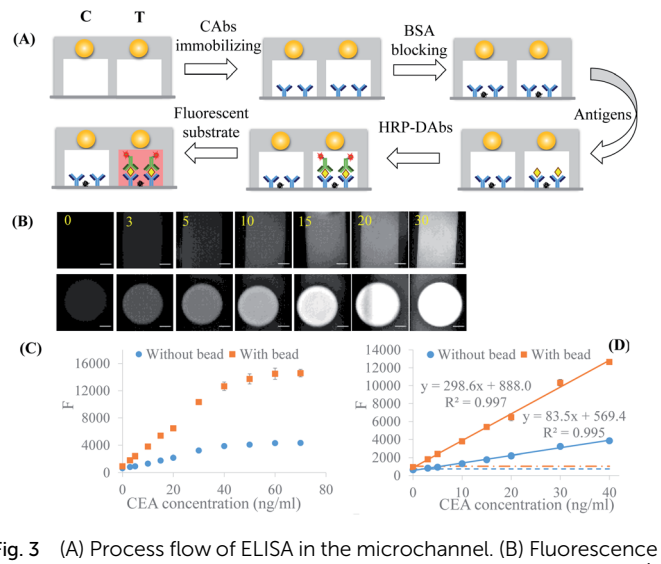

Fig. 3 (A) Process flow of ELISA in the microchannel. (B) Fluorescence images obtained from standard CEA solutions from 0 to 30 ng mL^{-1}. The top and bottom row represent original images in the absence of the bead and bead-enhanced images respectively. (C) Quantitative relationship of fluorescence intensity against CEA concentration. (D) Dynamic curves of CEA assay. The dotted lines represent the LODs of CEA measurement. Scale bars, 160 μm.

The limit of detection (LOD) of CEA measurement extrapolated from the blank value plus three-fold standard deviation was lowered ~3.1-fold and reached 0.68 ng mL^{-1}, which was comparable with other techniques (Table S1†). In comparison with the previous fluorescence-enhancing techniques, BFE effect was a contactless and effective method with no interference to immunoreaction and no modification of ELISA reagent. The improved detection sensitivity, the standard process flow, and the great automation potential would enable BFE microfluidic immunoassay be suitable for the clinical testing.

Evaluation of specificity and matrix effect

BSA, SCC, NSE, and PSA were used as interfering proteins to evaluate the specificity. The concentration of interfering proteins (100 ng mL^{-1}) was 5-fold higher than CEA concentration (20 ng mL^{-1}). In the absence of the bead, the fluorescence of interfering proteins was comparable with the blank value and appreciably lower than that of CEA, which verified the high specificity of ELISA. Based on BFE effect, all the fluorescence signals were increased, but the enhancing factor of CEA was remarkably greater than that of others. The enhanced fluorescence of interfering proteins was still in the same level with the enhanced blank value, and the gaps between CEA and interfering proteins were even bigger than those before enhancement (Fig. 4A). Therefore, BFE effect showed no damage to the specificity of ELISA.

Clinical samples, including plasma, serum, and cerebrospinal fluid, were usually complex. The matrix effect was inevitable. In this study, we diluted CEA-free plasma with different folds to test matrix effect. The background fluorescence of CEA-free plasma showed a remarkable decreasing when the dilution fold was varied from 0 to 2. The further dilution would not reduce the background signal (Fig. 4B). The clinical plasmas were diluted two folds in the subsequent experiments to suppress the background noise.

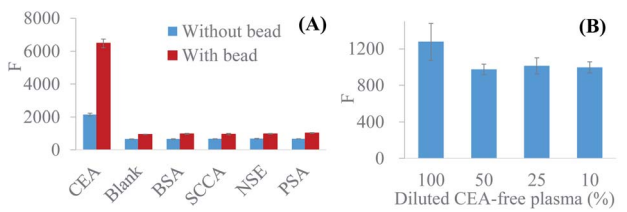

Fig. 4 (A) Evaluation of interfering proteins. (B) Matrix effect of plasma.

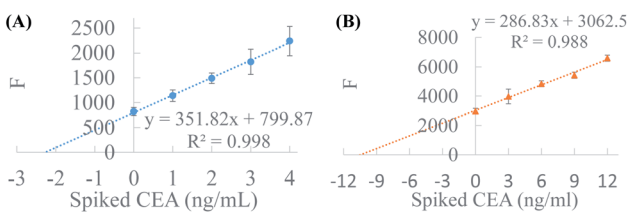

Fig. 5 The standard addition curves of 50% plasma. CEA negative plasma (A) and CEA positive plasma (B).

Clinical plasma measurement

CEA negative and positive plasma samples were detected using standard addition method. Fig. 5 showed the standard addition curves of these two plasmas with 2-fold dilution. The measured concentrations of normal and patient plasmas were 4.54 ng mL^{-1} and 21.35 ng mL^{-1} respectively, both of which were close to the standard values (3.77 and 25.48 ng mL^{-1}) provided by the hospital and fitted for the judgement of plasma. The recoveries of spiked CEA are varied in the range of 100.1% to 117% for CEA negative plasma and 91.0% to 111.4% for CEA positive plasma. The deviation between measured values and standard values might be caused by the RI variation of the bead and different resource of antibodies. The accurate analysis of normal and patient plasmas indicated that BFE base immunoassay could be applied for clinical sample detection.

Conclusions

In conclusion, we present a contactless and ball-lens assisted sensitivity improvement method for the fluorescence or luminescence immunoassay. BFE effect was evaluated from experiments and verified by the simulation. After optimization, the sensitivity of immunofluorescence detection of CEA was improved about 3.6-fold and the LOD was lowered more than 3-fold by BFE effect, meanwhile, BFE effect showed no weakening of the specificity and accuracy of ELISA. For plasma detection, the measured CEA concentration was very close to that provided by the hospital, demonstrating the potential of BFE effect in clinical testing. The established method is compatible with standard ELISA process, commercial reagent kit and automatic microfluidic immunoassay system, displaying a great potential in clinical application. On the other side, BFE effect can be coupled with other signal enhancing techniques (such as QD labelling and plasmon resonance), providing a probability of ultra-sensitive protein assay.

Ethic statement

Serum samples were collected form The Second Affiliated Hospital, Zhejiang University School of Medicine. All experiments were performed in accordance with the guidelines of clinical sample management rules of the hospital, and approved by the Ethics Committee at Jiangsu Normal University. Informed consents were obtained from human participants of this study.

Conflicts of interest

There are no conflicts to declare.

Acknowledgements

We are grateful to Dr Yong Wang at JSNU for his work on fluorescence enhancement simulation and helpful discussion. We thank Xuzhou key plan of R&D (KC20170) and Postgraduate Research and Practice Innovation Program of Jiangsu Province (KYCX20_2356) for funding of this project.

Notes and references

1 A. V. Lin, *Methods Mol. Biol.*, 2015, **1318**, 61–67.
2 D. A. Giljohann and C. A. Mirkin, *Nature*, 2009, **462**, 461–464.
3 W. Liu, L. Liu, G. Kou, Y. Zheng, Y. Ding, W. Ni, Q. Wang, L. Tan, W. Wu, S. Tang, Z. Xiong and S. Zheng, *J. Clin. Microbiol.*, 2020, **58**, e00461-20.
4 V. Roy, S. Fischinger, C. Atyeo, M. Slein, C. Loos, A. Balazs, C. Luedemann, M. G. Astudillo, D. Yang, D. R. Wesemann, R. Charles, A. J. Lafrate, J. Feldman, B. Hauser, T. Caradonna, T. E. Miller, M. R. Murali, L. Baden, E. Nilles and E. Ryan, *J. Immunol. Methods*, 2020, **484**, 112832.
5 L. Ma, A. Nilghaz, J. R. Choi, X. Liu and X. Lu, *Food Chem.*, 2018, **246**, 437–441.
6 L. Wu, G. Li, X. Xu, L. Zhu, R. Huang and X. Chen, *Trends Anal. Chem.*, 2019, **113**, 140–156.
7 K. Petropoulos, S. F. Bodini, L. Fabiani, L. Micheli, A. Porchetta, S. Piermarini, G. Volpe, F. M. Pasquazzi, L. Sanfilippo, P. Moscetta, S. Chiavarini and G. Palleschi, *Sens. Actuators, B*, 2019, **283**, 865–872.
8 G. Jaria, V. Calisto, M. Otero and V. I. Esteves, *Anal. Bioanal. Chem.*, 2020, **412**, 3983–4008.
9 Q. Zhang, X. Zhang, J. Li and H. Gai, *Anal. Chem.*, 2020, **92**, 654–658.
10 L. Cohen and D. R. Walt, *Annu. Rev. Anal. Chem.*, 2017, **10**, 345–363.
11 J. Zhang, J. M. Vernes, J. Ni, C. Nelson, A. Wong, S. T. Chen, A. Asundi, R. Vandlen and Y. G. Meng, *Anal. Biochem.*, 2014, **463**, 61–66.
12 M. S. Tabatabaei, R. Islam and M. Ahmed, *Anal. Chim. Acta*, 2021, **1143**, 250–266.
13 X. Liu, C. Huang, X. Dong, A. Liang, Y. Zhang, Q. Zhang, Q. Wang and H. Gai, *Chem. Commun.*, 2018, **54**, 13103–13106.
14 X. Liu, C. Huang, C. Zong, A. Liang, Z. Wu, Y. Zhang, Q. Zhang, W. Zhao and H. Gai, *ACS Sens.*, 2018, **3**, 2644–2650.
15 J. F. Li, C. Y. Li and R. F. Aroca, *Chem. Soc. Rev.*, 2017, **46**, 3962–3979.
16 Y. Jeong, Y. M. Kook, K. Lee and W. G. Koh, *Biosens. Bioelectron.*, 2018, **111**, 102–116.
17 V. Yelleswarapu, J. R. Buser, M. Haber, J. Baron, E. Inapuri and D. Issadore, *Proc. Natl. Acad. Sci. U. S. A.*, 2019, **116**, 4489–4495.
18 D. M. Rissin, C. W. Kan, T. G. Campbell, S. C. Howes, D. R. Fournier, L. Song, T. Piech, P. P. Patel, L. Chang, A. J. Rivnak, E. P. Ferrell, J. D. Randall, G. K. Provuncher, D. R. Walt and D. C. Duffy, *Nat. Biotechnol.*, 2010, **28**, 595–599.
19 J. Li, X. Zhao, L. J. Chen, H. L. Qian, W. L. Wang, C. Yang and X. P. Yan, *Anal. Chem.*, 2019, **91**, 13191–13197.
20 X. J. Liu, Y. Zhang, A. Liang, H. Ding and H. Gai, *Chem. Commun.*, 2019, **55**, 11442–11445.
21 D. T. Chiu, A. J. deMello, D. Di Carlo, P. S. Doyle, C. Hansen, R. M. Maceiczyk and R. C. R. Wootton, *Chem*, 2017, **2**, 201–223.
22 A. Chen, G. Fu, Z. Xu, Y. Sun, X. Chen, K. S. Cheng, K. H. Neoh, Z. Tang, S. Chen, M. Liu, T. Huang, Y. Dai, Q. Wang, J. Jin, B. Jin and R. P. S. Han, *Cancer Res.*, 2018, **78**, 4073–4085.
23 X. Yu, H. S. Xia, Z. D. Sun, Y. Lin, K. Wang, J. Yu, H. Tang, D. W. Pang and Z. L. Zhang, *Biosens. Bioelectron.*, 2013, **41**, 129–136.
24 J. T. Kindt, M. S. Luchansky, A. J. Qavi, S. H. Lee and R. C. Bailey, *Anal. Chem.*, 2013, **85**, 10653–10657.
25 H. Yang and M. A. M. Gijs, *Chem. Soc. Rev.*, 2018, **47**, 1391–1458.
26 F. Teng and M. Libera, *Langmuir*, 2018, **34**, 14969–14974.
27 J. J. Schwartz, S. Stavrakis and S. R. Quake, *Nat. Nanotechnol.*, 2010, **5**, 127–132.
28 H. Yang, M. Cornaglia and M. A. Gijs, *Nano Lett.*, 2015, **15**, 1730–1735.
29 H. Yang and M. A. Gijs, *Anal. Chem.*, 2013, **85**, 2064–2071.
30 J. Chen, X. Liu and Q. Zhang, *J. Micromech. Microeng.*, 2020, **30**, 047001.
31 Q. Zhang, J. Chen and H. Gai, *J. Mater. Sci.*, 2019, **54**, 14905–14913.
32 P. Ghenuche, J. d. Torres, P. Ferrand and J. e. o. Wenger, *Appl. Phys. Lett.*, 2014, **105**, 131102.
33 H. Zeng, D. Katagiri, T. Ogino, H. Nakajima, S. Kato and K. Uchiyama, *Anal. Chem.*, 2016, **88**, 6135–6139.
34 J. Kuo, C. Chiou and W. Lee, *J. Chin. Inst. Eng.*, 2012, **35**, 589–594.